Underlying catastrophes

Mike R. Jeffrey*

April 16, 2026

Abstract

Underlying catastrophes provide a method for locating bifurcation points of vector fields by providing solvable conditions to find points where stationary points collide, disregarding other dynamical features. Here I summarise these conditions, showing how they develop on Thom's catastrophe theory and the singularities of mappings. The method of finding underlying catastrophes is illustrated through some novel examples, including cases of coinciding saddle-node and saddle-focus bifurcations, and umbilic bifurcations. A gradient vector field that was given as an early refutation of Thom's catastrophe theory is reconsidered in this framework. The geometry of the unfoldings is explored for the underlying catastrophes up to codimension 4.

Contents

*School of Engineering Mathematics & Technology, University of Bristol, Ada Lovelace Building, Bristol, UK, email: mike.jeffrey@bristol.ac.uk

1 Introduction

The qualitative local forms of a mapping $f : \mathbb{R}^n \to \mathbb{R}^m$ are described by the incredibly general theory of *singularities of mappings* [3, 10, 19]. For local changes of a vector field $f : \mathbb{R}^n \to \mathbb{R}^n$ we have the theory of local *bifurcations of vector fields*. Both define classes of functions that are alike under certain equivalences, meant to characterise the order (or degeneracy) of the stationary points of f, but the theory of bifurcations of vector fields is both less complete and less practically wieldable than the theory of singularities of mappings. It is less complete because there is no general way to extend it to successively higher orders without case-by-case study, unlike the theory of singularities of mappings, and less practical because, except for a few of the most low order low dimensional cases, it lacks general conditions to detect any given bifurcation.

For systems with a gradient vector field $f = \nabla\phi$ in terms of a potential $\phi : \mathbb{R}^n \to \mathbb{R}$, Thom's theory of *catastrophes* provides something closer to the generality and simplicity of the singularities of mappings [22, 24, 25], dependent only on the geometry of the functions themselves rather than the topology of their integral curves, i.e. their dynamics.

In [13] I proposed a way of applying the geometrical simplicity of catastrophe theory to vector fields more generally, by stripping away the dynamics to reveal the catastrophe underlying it. This provides explicitly solvable conditions for finding a bifurcation point, for any dimension of system and any codimension of bifurcation. These *underlying catastrophes* do not constitute bifurcation classes themselves, but once they are found, one may then carry out local stability analysis to ascertain the precise bifurcation class. Here I will summarise the concept of underlying catastrophes of vector fields, what is known about them so far and the conditions to find them. To illustrate their role as organising centres of pattern formation I take a well understood example from optics, of the universal patterns formed by diffraction caustics around catastrophes.

René Thom was highly influential in the singularity theory of both mappings and gradient systems, and coincidentally, as I write, this year marks the 50^{th} anniversary of Thom's book *Structural stability and morphogenesis* being translated into English [25]. In particular Thom introduced the idea that, given a certain number of control parameters, one could determine exactly what local singularities could arise: these were the elementary catastrophes, listed in table 1 and illustrated in parameter space in fig. 1.

Thom intended that his catastrophes would classify all local changes of behaviour that could happen in a physical system as it changed with pa-

catastrophe	corank	codim-ension	class	unfolding of $V = \nabla\phi$
equilibrium			A_1	x
fold	1	1	A_2	$x^2 + \alpha_1$
cusp		2	A_3	$x^3 + \alpha_2 x + \alpha_1$
swallowtail		3	A_4	$x^4 + \alpha_3 x^2 + \alpha_2 x + \alpha_1$
butterfly		4	A_5	$x^5 + \alpha_4 x^3 + \alpha_3 x^2 + \alpha_2 x + \alpha_1$
...		k	A_k	$x^k + \alpha_k x^{k-2} + ... + \alpha_2 x + \alpha_1$
hyperbolic umbilic	2	3	D_4^+	$\begin{pmatrix} 3x_1^2 + \alpha_3 x_2 - \alpha_1 \\ 3x_2^2 + \alpha_3 x_1 - \alpha_2 \end{pmatrix}$
elliptic umbilic		3	D_4^-	$\begin{pmatrix} 3x_1^2 - 3x_2^2 + 2\alpha_3 x_1 - a \\ -6x_1 x_2 + 2\alpha_3 x_2 - \alpha_2 \end{pmatrix}$
parabolic umbilic		4	D_5	$\begin{pmatrix} 2x_1 x_2 + 2\alpha_3 x_1 - \alpha_1 \\ x_1^2 + 4x_2^3 + 2\alpha_4 x_2 - \alpha_2 \end{pmatrix}$
...		k	D_{k+1}	...
symbolic umbilic	2	5	E_6	$\begin{pmatrix} 3x_1^2 + 2\alpha_5 x_2^2 + \alpha_3 x_2 + \alpha_1 \\ 4x_2^3 + 2\alpha_5 x_1 x_2 + \alpha_3 x_1 + 2\alpha_4 x_2 + \alpha_2 \end{pmatrix}$
...		k	E_{k+1}	...

Table 1: Thom's elementary catastrophes. Initially Thom introduced just those up to codimension 4, which would unfold in the 'parameters' of 4-dimensional space and time [24], but class A_6 and A_7 also have names, the wigwam and star, respectively. The corank is essentially the minimum number of dimensions $(x_1, x_2, ...)$ for it to occur, the codimension is the number of parameters $(\alpha_1, \alpha_2, ...)$ needed to unfold it.

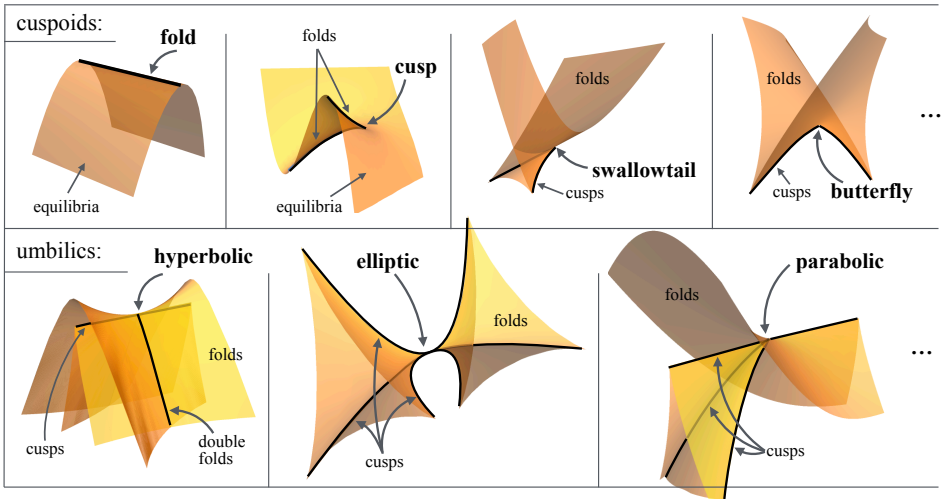

Figure 1: The elementary catastrophes up to codimension 4. The surfaces are the sets of *folds*, which crease along *cusps*, which themselves crease along *swallowtails* or umbilics, and so on. Shown in parameter space (or a projection thereof for codimension> 3).

rameters, but its limitation to systems governed by a gradient vector field $f = \nabla\phi$ narrows its usage outside fundamental physics. The difficulty of vector fields lies, of course, in how their dynamics depends on the topology of their orbits (integral curves), which can form connections between equilibria, limit cycles, and related higher dimensional invariant surfaces for $n \geq 3$; these are issues that do not inflict a mapping ϕ, nor a potential ϕ, though they may affect even a gradient field $f = \nabla\phi$ to a limited degree. This was, in fact, an objection to Thom's theory made by Guckenheimer in [11], citing an example of a gradient vector field that did not seem to lie within Thom's universal unfoldings, but I will show that this case actually lives within a larger class of bifurcations, one seemingly overlooked (despite Guckenheimer's observation) in subsequent bifurcation classifications. This class is important as it provides two ways for 4 equilibrium points of a vector field to collide, both fundamentally different from the swallowtail catastrophe (which also involves 4 equilibria colliding), even without taking into account objects like orbital connections between equilibria or limit cycles. They seem to be absent from the most complete classifications available, like Table 1 in [2].

Notwithstanding its issues, catastrophe theory remains the most evocative description of qualitative local change in nature. It is my aim with the concept of underlying catastrophes to bring the simplicity of those ideas back into bifurcation theory, and in particular use it to render bifurcation theory more amenable to application, without altering the theory itself.

Since we will use the terms singularity, bifurcation, and catastrophe, a brief comment on their meaning is warranted. A *singularity* is essentially a place where the rank of the Jacobian derivative of f is not maximal. *Bifurcations* are topological changes in f often seen at such a points as parameters vary smoothly, specifically topological changes in the flow of f when considering vector fields, and these are referred to as *catastrophes* if f is a gradient field $f = \nabla\phi$. An *underlying catastrophe* is a bifurcation only in the numbers of zeros of f, not concerned with the topology of its flow. A good book distinguishing the concepts more rigorously is [21].

I will first briefly review why a method to find bifurcations is needed. Even if one disregards the vectorial nature of a function f and treats it more simply as a mapping, the number of conditions needed to characterise its singularities are potentially enormous, as described in section 2 via the Thom-Boardman procedure. The conditions introduced in [13] to define underlying catastrophes are then summarised in section 3, before applying them to various examples in the remainder of the paper, highlighting some particularly novel cases, and showing both the methodology and weaknesses

of the method. We begin with the simple folds in section 4, comparing saddle-node and saddle-focus cases. Section 5 shows that there are three fundamentally different mechanisms by which 4 equilibria of a vector field can bifurcate, even without taking into account their stability, namely via swallowtail catastrophes and the more exotic umbilic catastrophes, including the example given as an early objection to Thom's catastrophe theory. Unfoldings of the underlying catastrophes up to codimension 4 are given in section 6, with some closing remarks in section 7.

In examples we will always consider an ordinary differential equation $\dot{x} = f(x)$, in the plane for ease of illustration, but the results here extend directly to higher dimensions, and also to more general differential equations such as a higher order ordinary differential equation like $\ddot{x} = f(x)$, or even a partial differential equation like $\frac{\partial}{\partial t}x = \frac{\partial^2}{\partial^2 u}x + f(x)$ where $u \in \mathbb{R}^p$ is some spatial variable, for examples see [1, 13, 14, 15].

2 Classification: The number problem

General methods for finding a singularity or bifurcation of a dynamical system are surprisingly lacking. Perhaps the most general is the Thom-Boardman classification, which is an algebraic procedure provided by Boardman to capture Thom's geometrical arguments of versality, providing an infinite classification of singularities that was later formalised further through the language of ideals [6, 20]. The rigour and generality of this period of singularity theory could be ranked among the most profound achievements of mathematics, yet it is less widely known than perhaps it could be in the field of dynamical systems.

The Thom-Boardman procedure classifies singularities by taking a vector field and calculating a sequence of minors of its derivatives, then the minors of their derivatives, and so on. The growth of the number of calculations is shown in table 2, from a formula given in an appendix of [14]. For a system of dimension n, and singularity of codimension r, it involves a nested sum of factorials of sums of factorials etc. of n and r, such that even an asymptotic approximation so far evades imagination.

More precisely, given a function $f : \mathbb{R}^n \to \mathbb{R}^n$ (the general procedure can be defined for mappings $\mathbb{R}^n \to \mathbb{R}^m$ but for vector fields we require only $\mathbb{R}^n \to \mathbb{R}^n$), the *Boardman symbol* of f at some point $x = 0$ is a string $\tau = \tau_1, ..., \tau_r$, where the symbols $\tau_1, ..., \tau_r$, form a non-increasing sequence $\tau_1 \geq \tau_2 \geq ... \geq \tau_r$. Each τ_j is the corank of a matrix $\nabla\Delta^{\tau_{j-1}}...\Delta^{\tau_1}f$, and the symbol τ is taken to terminate at r such that $\tau_{r+1} = 0$. These matrices $\nabla\Delta^{\tau_{j-1}}...\Delta^{\tau_1}f$

characterise the degeneracy of the singularity at each order j. The first matrix is $\Delta^1 f = (f, \det \nabla f)$, and more generally for $i_1 > 1$ we let $\Delta^{i_1} g = \left(g, m_1^{i_1}, m_2^{i_1}, ...,\right)$, where $m_j^{i_1}$, $j = 1, ..., N_1$, are the $(n - i_1 + 1) \times (n - i_1 + 1)$ minors of ∇f. Successive orders are obtained iteratively by taking minors of the previous matrix, so next we define $\Delta^{i_2}\Delta^{i_1} f = \left(\Delta^{i_1} f, m_{2,1}^{i_2}, m_{2,2}^{i_2}, ...\right)$, where $m_{2,j}^{i_2}$ are the $(n - i_2 + 1) \times (n - i_2 + 1)$ minors of $\nabla(\Delta^{i_1} f)$, then $\Delta^{i_3}\Delta^{i_2}\Delta^{i_1} f = \left(\Delta^{i_2}\Delta^{i_1} f, m_{3,1}^{i_3}, m_{3,2}^{i_3}, ...\right)$, where $m_{3,j}^{i_3}$ are the $(n - i_3 + 1) \times (n - i_3 + 1)$ minors of $\nabla(\Delta^{i_2}\Delta^{i_1} f)$, and so on iteratively, giving for any j,

$$\Delta^{i_j} ... \Delta^{i_1} f = \left(\Delta^{i_{j-1}} ... \Delta^{i_1} f, m_{j,1}^{i_j}, m_{j,2}^{i_j}, ...\right) \ , \tag{1}$$

where $m_{j,k}^{i_j}$ for $k = 1, ..., N_j$, are the $(n - i_j + 1) \times (n - i_j + 1)$ minors of $\nabla(\Delta^{i_{j-1}} ... \Delta^{i_1} f)$. While the procedure can be written concisely like this, it is evidently lengthy. In fact, the total number of these minors grows at an incredible rate with a systems's dimension n (its number of variables) and the singularity's codimension r (its number of control parameters). A formula for the number of minors to be calculated was given [14], and the first few are shown in table 2.

codim. $r = \rightarrow$ dim. $n = \downarrow$	1	2	3	4	5
1	2	4	8	16	32
2	3	6	21	231	26796
3	4	8	64	41728	12×10^{12}
4	5	10	220	94967015	3×10^{30}

Table 2: The number problem: the number of minors calculated to identify a singularity in the Thom-Boardman procedure, up to dimension $n = 4$ and codimension $r = 5$.

Of course, no system can typically satisfy such a huge number of conditions, even before we begin to take into account additional conditions needed to identify bifurcations organised around such singularities in vector fields. So these may provide a means to classify a singularity, but not a practical method to locate one in either a mapping or a vector field.

In the normal approach to vector fields, to find bifurcations we must find its equilibria, then study either eigenvalues or derivatives of f vanish at these equilibria, or integrals along orbits vanish to indicate close cycles or connections. For brute force numerical detection or continuation methods, the conditions that must be solved are known only for low dimension and codimension. Analytically the only general procedure is to reduce first to

a normal form along the centre manifold of the bifurcation, but then this requires, of course, finding where that bifurcation occurs first.

Many of the conditions enumerated in table 2 turn out to be either trivially zero or equivalent, but the manner of their independence is not obvious. In [14] it was shown under certain restrictions that they can be reduced to the minimum possible number of conditions that could define a singularity: the number of variables n plus the number of parameters r required to unfold it, shown in table 3. This is achieved via the '$\mathcal{B}$-$\mathcal{G}$ conditions' defining the *underlying catastrophes*, given in the next section.

codim. $r = \rightarrow$ dim. $n = \downarrow$	1	2	3	4	5
1	2	3	4	5	6
2	3	4	5	6	7
3	4	5	6	7	8
4	5	6	7	8	9

Table 3: The number of $\mathcal{B}$ determinants needed to identify an underlying catastrophe, up to dimension $n = 4$ and codimension $r = 5$, as calculated in [14].

3 The $\mathcal{B}$-$\mathcal{G}$ conditions for underlying catastrophes

Underlying catastrophes are essentially a way of applying contact equivalence to vector fields. They describe the contact between zero sets of different functions, namely here the zeros of a vector field and its derivatives, and neglecting anything else like dynamics or orbital equivalence. I will summarise the conditions defining underlying catastrophes below for use later in the paper.

Let us write $f = (f_1, ..., f_n)$, depending on a variable $x = (x_1, ..., x_n)$ and parameter $\alpha = (\alpha_1, ..., \alpha_p)$. Denote the derivative operator over x as $\nabla = \frac{\partial}{\partial x}$ and over (x, α) as $\square = \left(\frac{\partial}{\partial x}, \frac{\partial}{\partial \alpha}\right)$. We assume the singularity or bifurcation of interest occurs at some $(x, \alpha) = (x_*, \alpha_*)$, and give conditions below to find this point.

A singularity of a vector field occurs where the Jacobian determinant $|\nabla f|$ vanishes, and then the first quantity defining that singularity is its *corank*.

Let us first assume the corank of ∇f is one, and that any set of $n-1$ of the gradient vectors ∇f_i *are* linearly independent, defined as the 'subrank' of f being $n-1$ in [14].

Instead of the minors of the Thom-Boardman procedure in section 2, we can then define a sequence of determinants

$$\mathcal{B}_1 = |\nabla(f_1, f_2, ..., f_n)| \quad \text{and} \quad \mathcal{B}_i = |\nabla(\mathcal{B}_{i-1}, f_2, ..., f_n)| \ . \tag{2}$$

So $\mathcal{B}_1$ is the Jacobian of f, and each $\mathcal{B}_i$ is obtained from the previous one by substituting $\mathcal{B}_{i-1}$ in place of the first component of f. An *underlying catastrophe* of codimension r is then defined by the conditions

$$0 = f = \mathcal{B}_1 = \mathcal{B}_2 = ... = \mathcal{B}_r \ . \tag{3}$$

The cases $r = 1, 2, 3, ...$ correspond to Thom's elementary catastrophes in table 1, and are named as such: the fold ($r = 1$), cusp ($r = 2$), swallowtail ($r = 3$), etc. The system (3) only has unique solutions (x_*, α_*) if the catastrophe is 'full', which means a further set of determinants $\mathcal{G}_{r,k_1...k_{i-1}}$ are nonzero for all $k_1, ..., k_{i-1} \in \{1, ..., n\}$. These are functions

$$\mathcal{G}_{i,K(i)} = \left|\Box\left(f_1, ..., f_n, \mathcal{B}_1, ..., \mathcal{B}_{i,K(i)}\right)\right| \ , \tag{4}$$

where $K(i)$ denotes the index string $K(i) = k_1...k_{i-1}$, and where the functions $\mathcal{B}_{i,K(i)} \equiv \mathcal{B}_{i,k_1...k_{i-1}}$ are determinants

$$\mathcal{B}_{i,K(i)} = \left|\nabla\left(f_1, ..., f_{h-1}, \mathcal{B}_{i-1,K(i-1)}, f_{h+1}, ..., f_n\right)\right| \ , \tag{5}$$

with $h = k_{i-1}$. These are more numerous than the $\mathcal{B}$ conditions, but one needs only calculate them to ensure they are non-vanishing.

If the corank of ∇f is two then we obtain the umbilics. Assume then that any $n-2$ of the gradient vectors $\nabla f_1, ..., \nabla f_n$, are linearly independent. To characterise these we are interested first in minors of ∇f of dimension $n-1$. For convenience let us denote a vector v with the j^{th} component deleted by $v_{-j} = (v_1, ..., v_{j-1}, v_{j+1}, ..., v_n)$, then we can write these minors as

$$\mathcal{B}^2_{1,k} = \left|\frac{\partial f_{-u}}{\partial x_{-v}}\right| \ , \qquad \begin{array}{l} k = v + (u-1)n, \\ u, v = 1, ..., n. \end{array} \tag{6}$$

The first umbilic catastrophe then occurs at a point (x_*, α_*) where

$$\mathcal{B}^2_{1,1} = \mathcal{B}^2_{1,2} = \mathcal{B}^2_{1,3} = \mathcal{B}^2_{1,4} = 0 \ , \tag{7}$$

and these are 'full' provided that all

$$\mathcal{G}^2_{1,k_1k_2k_3k_4} = \left|\left(\Box\left(f_1, ..., f_n, \ \mathcal{B}^2_{1,k_1}, \ \mathcal{B}^2_{1,k_2}, \ \mathcal{B}^2_{1,k_3}, \ \mathcal{B}^2_{1,k_4}\right)\right)\right| \ , \tag{8}$$

are non-vanishing for all $k_1, k_2, k_3, k_4 \in 1, ..., n^2$ with $k_1 \neq k_2 \neq k_3 \neq k_4$. The umbilics can be of *hyperbolic* or *elliptic* type, as I will describe in section 5 and section 6. Note that as we require 4 conditions in (7), these umbilic catastrophes are of codimension 4, in contrast to gradient systems in Thom's theory where they are codimension 3 (see table 1). We will see in section 5 how this helps resolve the Guckenheimer objection mentioned in section 1.

One may continue to higher codimension umbilics, involving determinants of the form

$$\mathcal{B}^2_{2,k_1k_2} = \left|\nabla \left(\mathcal{B}^2_{1,k_1},\ \mathcal{B}^2_{1,k_2},\ f_3, ..., f_n\right)\right| \ , \tag{9}$$

however little work has so far been carried out for higher codimension umbilics, either in the elementary or underlying catastrophes. Finding the underlying catastrophes corresponding to the known parabolic and symbolic umbilic catastrophes remains to be done.

If one then conjectures that a system undergoes a bifurcation, at unknown values of the variable x and parameter α, then using the $\mathcal{B}$-$\mathcal{G}$ conditions of the underlying catastrophe one can find its location, and then begin a local stability analysis to fully determine its bifurcation class. The method is essentially:

(i.) Solve the conditions $f = 0$ to identify families of equilibria; rather than solving for the variables $(x, y, ...)$, it can be better to solve for some subset of the parameters $(\alpha_1, \alpha_2, ...)$ parameterised by $(x, y, ...)$, as we will use in section 5.

(ii.) Solve $\mathcal{B}_1 = 0$ along with (i.) to identify families of folds, checking that $\mathcal{G}_1 \neq 0$ on these solutions, to ensure non-degeneracy. One may have to choose which parameter to consider $\mathcal{G}_1$ with respect to, as only certain parameters may unfold the catastrophe non-degenerately.

(iii.) Solve $\mathcal{B}_2 = 0$ along with (i-ii.) to identify families of cusps, checking that $\mathcal{G}_{2,k} \neq 0$ for $k = 1, 2, ...n$ on these solutions. Again one may have to choose which 2 parameters to consider $\mathcal{G}_1$ and $\mathcal{G}_{2,k}$ with respect to.

(iv.) Continue to $\mathcal{B}_3$ for a swallowtail or $\mathcal{B}^2_{1,k}$ for an umbilic, and so on to successive orders until all catastrophes have been found. At any order of interest, one may then conduct local stability analysis to study the local dynamics and identify the bifurcation class.

While one must ascertain appropriate parameters to unfold any given catastrophe, provided the non-degeneracy conditions $\mathcal{G}_{i,k_1...k_{i-1}} \neq 0$ hold, then the underlying catastrophe is *full*, the equations $f = \mathcal{B}_1 = ... = \mathcal{B}_r = 0$ have well-defined solutions independent of the choice of coordinates. Moreover in (2) we choose a certain form for the $\mathcal{B}_i$ where each $\mathcal{B}_{i-1}$ replaces the first component of f in calculating the next $\mathcal{B}_i$ – one may equivalently

choose to replace a different component of f, e.g. if this simplifies the calculations, without altering the result. If the conditions $\mathcal{G}_{i,k_1\ldots k_{i-1}} \neq 0$ do not hold, then a small perturbation or change of coordinates may restore them, however little work has been done in studying such cases to date.

In the following sections we investigate some of the vector field bifurcations revealed by underlying catastrophes, including cases that are absent from standard bifurcation theory literature.

4 Underlying folds: beyond the saddle-node

To illustrate the alternative view that underlying catastrophes bring to bifurcation theory, let me begin with the simplest bifurcation of a vector field, the saddle-node, and its *underlying* relation to higher order bifurcations called the *nilpotents*, which start with the Bogdanov-Takens bifurcation.

Take a saddle-node in a planar system,

$$f = (x_1^2 + \alpha, x_2) \; . \tag{10}$$

As the parameter α changes from negative to positive, a pair of equilibria at $x = \pm\sqrt{-\alpha}$, one a saddle and one a node, collide and annihilate. In terms of the $\mathcal{B}$-$\mathcal{G}$ conditions from section 3, at $x = \alpha = 0$ this satisfies $f = \mathcal{B}_1 = 0$ and $\mathcal{G}_1 = 2 \neq 0$, hence it defines a full underlying fold.

Compare this to the form

$$f = (x_2, x_1^2 + \alpha) \; , \tag{11}$$

which yields again, as the parameter α changes from negative to positive, a pair of equilibria at $x = \pm\sqrt{-\alpha}$, one a saddle and one a *focus* this time, that collide and annihilate. Again in terms of the $\mathcal{B}$-$\mathcal{G}$ conditions, at $x = \alpha = 0$ this satisfies $f = \mathcal{B}_1 = 0$ and $\mathcal{G}_1 = -2 \neq 0$, so it too defines a full underlying fold. However, this saddle-focus event does not define a bifurcation class, requiring one extra parameter to fully unfold it, namely in the form of the Bogdanov-Takens bifurcation

$$f = (x_2, x_1^2 + \alpha_1 + \alpha_2 x_1 \pm x_1 x_2) \; , \tag{12}$$

which is in fact the first in a whole sequence of nilpotent bifurcations [9].

From the viewpoint of their underlying catastrophes, however, the saddle-node and saddle-focus (or Bogdanov-Takens in the case of (11)) are one and the same, simply an *underlying* fold. Both occur where two equilibria coincide, irrespective of any other dynamics going on around them.

Obviously it is easy to identify the site of any bifurcation in the examples above. Consider instead the system

$$f = \begin{pmatrix} (1-x_1)\,(\alpha_2 + (\alpha_2 + x_2 + 2x_1)x_2) + 3x_1 - x_2 - 2\alpha_1 x_2 - 2 \\ (1-x_1)\,(2 - \alpha_2 - x_1 + (1 - \alpha_2 - x_1 - x_2)x_2) + \alpha_1 x_1 + \alpha_1 \end{pmatrix} , \tag{13}$$

which has up to 6 equilibria, and therefore we cannot generally expect to find them analytically (though in this contrived case it turns out we can), nor is it obvious how to identify any bifurcations that might occur. Instead let us look for underlying catastrophes, working through the codimensions $r = 1, 2, ...$, though here we will need only $r = 1$. The condition for underlying folds is simply to find where f and its Jacobian determinant $\mathcal{B}_1$ vanish. There are a number of solutions, but only three of them are 'full' and hence non-degenerate, those at

$$(x_1, x_2, \alpha_1) \;=\; (0, -1, 0)\;,\;\; (0, 2 - \alpha_2, 0)\;,\;\; \text{and}\;\; (1 - \tfrac{1}{2}\alpha_2, 1, \tfrac{1}{4}\alpha_2^2)\;. \tag{14}$$

All of these are underlying folds that occur as α_1 changes. For $\alpha_2 = 0$ all three occur at $\alpha_1 = 0$, at different coordinates (x_1, x_2), with the former being a saddle-node and the latter two being Bogdanov-Takens (saddle-focus) bifurcations (which unfold fully in both parameters α_1, α_2, as the reader may verify by standard local stability analysis). Figure 2 shows all three catastrophes occurring simultaneously for $\alpha_2 = 0$ as α_1 changes sign.

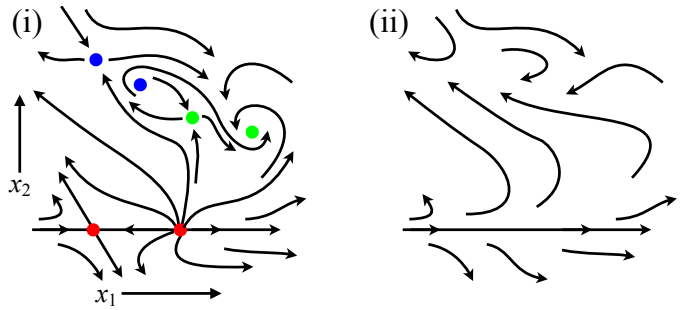

Figure 2: Folds occurring in the system $(\dot{x}_1, \dot{x}_2) = f$ with (13), as α_1 changes value with $\alpha_2 = 0$, showing: (i) for $\alpha_1 < 0$ the existence of a saddle-node pair (red), and two saddle-focus pairs (blue and green), (ii) for $\alpha_1 > 0$ no equilibria.

As low codimension events these bifurcations themselves are well categorised, but as we move to higher codimensions we enter less well understood ground. In the next section we look at three mechanisms that unfold 4 equilibria in the plane, one involving 3 parameters and two involving 4 parameters.

5 Swallowtails and Umbilics

Bifurcations of codimension greater than 2 are not often discussed in bifurcation theory texts, but they are certainly important in engineering and biological applications, where a nonlinear system of multiple dimensions and numerous parameters may easily exhibit multiple equilibria.

When one encounters a system with 4 or more equilibria, there are three fundamentally different ways they may collide, examples of which will be given below. I will state results on the type and stability of these equilibria without proof, which involve only linear stability analysis and so are theoretically standard, but would be lengthy as they involve quartic systems. (Note in the counts of equilibria described above we include multiplicity, i.e. two coincident equilibria are counted as two, not one.)

The first case to consider is the *swallowtail*, a bifurcation that occurs along a one dimensional centre manifold. This case is a direct extension of the saddle-node and cusp bifurcations in standard texts, e.g. [18], and appears in general classifications like Table 1 of [2]. It unfolds in the 3 parameters $(\alpha_1, \alpha_2, \alpha_3)$, over which it can have 0, 2, or 4, equilibria: two will be saddles, and two will be nodes with the same stability. An example is

$$f = \left(\alpha_2 + \alpha_1 x_1 + x_2 + x_1^3,\ \alpha_3 + x_1 + x_2^2\right) \ . \tag{15}$$

Let us use the conditions (2) to locate its catastrophes. We can solve the conditions (3) for each value of r, checking that the functions $\mathcal{G}_{r,k_1 \ldots k_{i-1}}$ are non-vanishing at each codimension. More useful geometrically can be to seek the catastrophe sets in the parameter space of $(\alpha_1, \alpha_2, \alpha_3)$ as follows. The equilibria lie on an (x_1, x_2, α_1)-parameterised set found, solving $f = 0$, as

$$(\alpha_2, \alpha_3) = -\left(\alpha_1 x_1 + x_2 + x_1^3,\ x_1 + x_2^2\right) \ .$$

Folds lie on surfaces found by solving $\mathcal{B}_1 = 2x_2(\alpha_1 + 3x_1^2) - 1 = 0$, where

$$\alpha_1 = (1 - 6x_1^2 x_2)/2x_2 \ ,$$

and these form cusps, solving $\mathcal{B}_2 = 24x_1x_2^2 - 6x_1^2 - 2\alpha_1 = 0$, along curves where

$$\mathcal{B}_2 = 0 \qquad \Rightarrow \qquad x_1 = 1/24x_2^3 \ .$$

Finally, solving $\mathcal{B}_3 = 0$, a swallowtail bifurcation is found to lie at the point

$$(x_1, x_2, \alpha_1, \alpha_2, \alpha_3) = (\tfrac{1}{2^{3/5}3}, \tfrac{1}{2^{4/5}}, \tfrac{5}{2^{6/5}3}, -\tfrac{35}{2^{4/5}27}, -\tfrac{5}{2^{8/5}3}) \ , \tag{16}$$

where we find $\mathcal{G}_{3,k_1k_2} = 720$ for all $k_1, k_2 \in \{1, 2\}$. Simulations of the phase portraits showing the different numbers and types of equilibria are given in fig. 3.

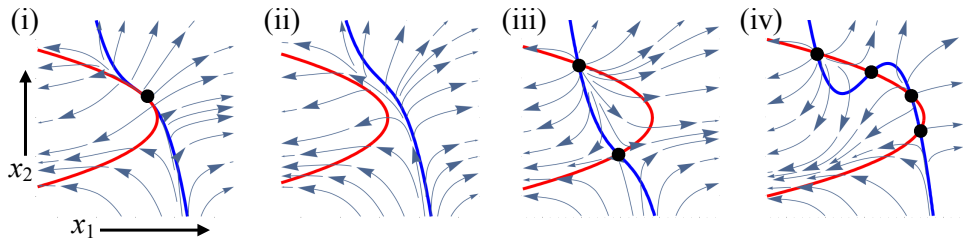

Figure 3: Phase portraits of the system $(\dot{x}_1, \dot{x}_2) = f$ given by (15) around a swallowtail bifurcation showing: (i) the swallowtail, (ii) 0 equilibria, (iii) 2 equilibria, (iv) 4 equilibria. Parameter values $(\alpha_1, \alpha_2, \alpha_3)$ are: (i) as in (16), (ii) $(1, -1, -0.2)$, (iv) $(1, 1, -0.8)$, (iv) $(-1, -1, -1.5)$. Showing nullclines of $f_1 = 0$ (blue curves) and $f_2 = 0$ (red curves).

But there are also two very different mechanisms by which four equilibria can bifurcate, related to *umbilics*. The umbilics are well known in singularity theory or in Thom's elementary catastrophes, but have never been properly classified in vector fields. They were shown to occur as *underlying umbilics* in [15], where an example was given of the *hyperbolic umbilic*, here we will show both *hyperbolic* and *elliptic* cases, again both are very different.

We can obtain a hyperbolic umbilic by changing (15) only slightly, reducing the cubic term to a quadratic, and augmenting the linear term to

$$f = \left(\alpha_2 + \alpha_1 x_2 + x_1^2,\ \alpha_3 + \alpha_4 x_1 + x_2^2\right) \ . \tag{17}$$

Similarly to above, but now in $(\alpha_1, \alpha_2, \alpha_3, \alpha_4)$ parameter space, we can find the equilibria as $(x_1, x_2, \alpha_1, \alpha_4)$-parameterised families

$$(\alpha_2, \alpha_3) = -\left(\alpha_1 x_2 + x_1^2,\ \alpha_4 x_1 + x_2^2\right) \ ,$$

which undergo folds on surfaces where $\mathcal{B}_1 = 0$, giving

$$\alpha_4 = 4x_1 x_2/\alpha_1 \ ,$$

and these crease along cusps on a curve where $\mathcal{B}_2 = 0$, giving

$$\alpha_1 = 2x_1^2/x_2 \ .$$

Finally these intersect at the hyperbolic point, where $\mathcal{B}^2_{1,k} = 0$ for $k = 1, 2, 3, 4$, (these are just the four components of the Jacobian), at

$$(x_1, x_2, \alpha_1, \alpha_2, \alpha_3, \alpha_4) = 0 \ ,$$

along with $\mathcal{G}^2_{1,1234} = 4$. Hence the hyperbolic umbilic unfolds over the 4 parameters $(\alpha_1, \alpha_2, \alpha_3, \alpha_4)$, over which it can have 0, 2, or 4, equilibria, like the swallowtail, but unlike the swallowtail: two will be saddles, and two will be nodes or foci with *opposing* stability. Simulations of the phase portraits showing the different numbers and types of equilibria are given in fig. 4.

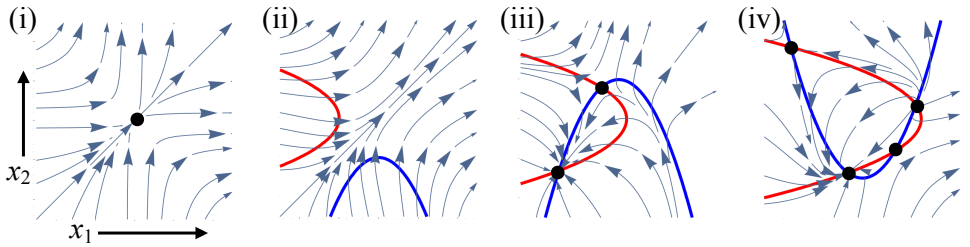

Figure 4: Phase portraits of the system $(\dot{x}_1, \dot{x}_2) = f$ given by (17) around a hyperbolic umbilic bifurcation showing: (i) the umbilic, (ii) 0 equilibria, (iii) 2 equilibria, (iv) 4 equilibria. Parameter values $(\alpha_1, \alpha_2, \alpha_3, \alpha_4)$ are: (i) $(0, 0, 0, 0)$, (ii) $(1, 1, 1, 1)$, (iv) $(1, -1, -0.2, 1)$, (iv) $(-1, -1.5, -1.5, 1)$.

We can obtain an elliptic umbilic by again changing (17) only slightly, adding $x_1 x_2$ terms as

$$f = \left(\alpha_2 + \alpha_1 x_2 + x_1^2 + x_1 x_2,\ \alpha_3 + \alpha_4 x_1 + x_2^2 + 2 x_1 x_2\right) \ . \tag{18}$$

Seeking its catastrophe surfaces in $(\alpha_1, \alpha_2, \alpha_3, \alpha_4)$ parameter space, its families of equilibria lie on $(x_1, x_2, \alpha_1, \alpha_4)$-parameterised families

$$(\alpha_2, \alpha_3) = -\left(\alpha_1 x_2 + x_1^2 + x_1 x_2,\ \alpha_4 x_1 + x_2^2 + 2 x_1 x_2\right) \ ,$$

which undergo folds on surfaces where $\mathcal{B}_1 = 0$, giving

$$\alpha_4 = 2(x_1 - \alpha_1 x_2 + (x_1 + x_2)^2)/(\alpha_1 + x_1) \ ,$$

and these crease at cusps along curves where $\mathcal{B}_2 = 0$, giving

$$\alpha_1 = (x_1^2 + 3 x_1 x_2 + \tfrac{3}{2} x_2^2)/(3 x_1 + 2 x_2) \ .$$

Lastly, these intersect at the elliptic point, where $\mathcal{B}^2_{1,k} = 0$ for $k = 1, 2, 3, 4$, at

$$(x_1, x_2, \alpha_1, \alpha_2, \alpha_3, \alpha_4) = 0 \ ,$$

along with $\mathcal{G}^2_{1,1234} = 2$. Again the bifurcation unfolds over the 4 parameters $(\alpha_1, \alpha_2, \alpha_3, \alpha_4)$, but unlike the previous cases it can only have 2 or 4 equilibria, and moreover: one is a saddle, and three are nodes or foci not all with the same stability (by altering signs in (18) one can also obtain the case of one node or focus and three saddles). Simulations of the phase portraits showing the different numbers and types of equilibria are given in fig. 5.

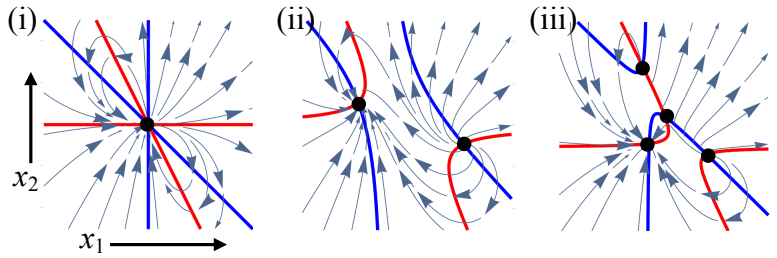

Figure 5: Phase portraits of the system $(\dot{x}_1, \dot{x}_2) = f$ given by (18) around an elliptic umbilic bifurcation showing: (i) the umbilic, (ii) 2 equilibria, (iii) 4 equilibria. Parameter values $(\alpha_1, \alpha_2, \alpha_3, \alpha_4)$ are: (i) $(0, 0, 0, 0)$, (ii) $(0.5, -1, 1, 0)$, (iii) $(0.4, -0.1, -0.1, 1)$.

I give a more detailed description of the unfoldings of these catastrophes in the next section. First let me remark on the counter-argument to Thom's catastrophe theory mentioned in section 1.

In [11], Guckenheimer gives the example of the potential system

$$\begin{aligned} \phi &= \tfrac{1}{3}(x_1^2 + x_2^2) + \alpha_1 x_1 x_2 + \alpha_2 x_1 + \alpha_3 x_2 \quad s.t. \\ f = \nabla\phi &= \left(\alpha_2 + \alpha_1 x_2 + x_1^2,\ \alpha_3 + \alpha_1 x_1 + x_2^2\right) \ , \end{aligned} \tag{19}$$

which we observe is almost the case (17), but with only 3 parameters. This example was given to show that Thom's classification of unfoldings of potentials ϕ was inadequate to classify even gradient vector fields $f = \nabla\phi$. The argument is that arbitrarily close to (19) lies another gradient system,

$$f = \nabla\left(\tfrac{1}{3}(x_1^2 + x_2^2) + \alpha_1 x_1 x_2 + \alpha_2 x_1 + \alpha_3 x_2 + \mu x_1^2 x_2\right) \ , \tag{20}$$

which for $\alpha_1 = \alpha_2 = 0$ and $\mu < 0$ has saddle connections, unlike (19). By a geometrical argument about universality, apparently too "tedious" to give in [11], this implies that, even in the family of gradient vector fields, this example should be of codimension 4, not 3 as in Thom's theory. The system (20) is shown with these saddle connections in fig. 6(i), and under perturbation in (ii).

Treating this using the $\mathcal{B}$-$\mathcal{G}$ conditions from section 3, the Jacobian components all vanish, i.e. $\mathcal{B}^2_{1,k} = 0$ for $k = 1, 2, 3, 4$. However, the 'fullness'

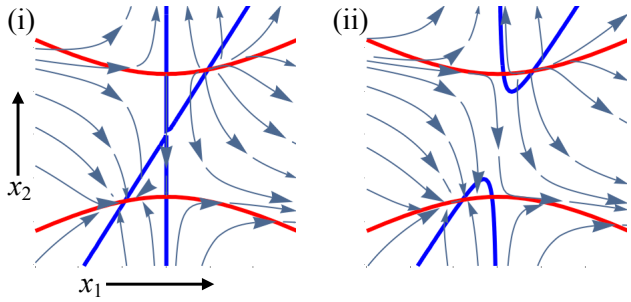

Figure 6: Phase portraits of the system (20) for $\alpha_1 = 0$, $\alpha_3 = -2$, $\mu = -1$, and (i) $\alpha_2 = 0$, (ii) $\alpha_2 = 1/2$.

condition fails as $\mathcal{G}^2_{1,1234} = 0$ for both (19) and (20), so this remains an unstable case. To obtain a full umbilic let us instead add Guckenheimer's '$+\mu x_1^2 x_2$' gradient perturbation to the full system (17), giving

$$f = \left(\alpha_2 + \alpha_1 x_2 + x_1^2 + 2\mu x_1 x_2,\ \alpha_3 + \alpha_4 x_1 + x_2^2 + \mu x_1^2\right) \ . \qquad (21)$$

Indeed this satisfies the umbilic conditions $\mathcal{B}^2_{1,k} = 0$ but now with $\mathcal{G}^2_{1,1234} = 4$, i.e. a full system. Note that this only remains a hyperbolic umbilic for $\mu > -1/4^{1/3}$, otherwise it is elliptic; I will give the conditions distinguishing the two this in the next section.

The outcome is that recognising these as *underlying umbilics* to some extent resolves the objection to Thom's catastrophes raised by Guckenheimer. The implication is subtle: while Thom's theory correctly classifies the catastrophes of potentials ϕ, determining the forms taken by their gradient vector fields $f = \nabla\phi$, it does *not* provide a complete classification of the vector fields f themselves, gradient or otherwise. We can, however, use Thom's theory to define the underlying catastrophes of vector fields, and while (19) has codimension 3 with respect to the catastrophes of the potential ϕ, it has codimension 4 with respect the underlying catastrophes of the vector field f.

6 Unfoldings of underlying catastrophes

To demonstrate how the $\mathcal{B}$-$\mathcal{G}$ conditions may be used to study underlying catastrophes of vector fields, highlighting the differences from bifurcation theory or elementary catastrophe theory, let me run through the elementary cases here, again using planar vector fields for ease of illustration. I will consider both corank 1 and corank 2, taking non-gradient vector fields in each case.

The bifurcation sets will be represented by showing the fold and higher catastrophe sets in parameter space. Phase portraits of the system $(\dot{x}_1, \dot{x}_2) = f$ will be shown, illustrating the types of equilibria that arise from each catastrophe, showing cases both reducible and non-reducible to one-dimensional centre manifolds by interchanging the components of f as $(f_1, f_2) \leftrightarrow (f_2, f_1)$, which does not affect the type of underlying catastrophe but can result in a higher codimension bifurcation class.

There are many possible applications where catastrophe theory could help explain bifurcation structures of vector fields, not only to ordinary differential equations like $(\dot{x}_1, \dot{x}_2) = f$. Examples of reaction-diffusion (partial differential equations) were given in [13, 14, 15], based on particular applications to biological cell models or chemical reactions in e.g. chemical reaction models in [1, 7, 8, 12, 23]. As an alternative, and better understood, illustration of the organising properties of the catastrophes, I will show simulations of light scattering from surfaces exhibiting Thom's catastrophes. These are simulated here by wave integrals of the form $\int_{\infty}^{+\infty} dx \cos(4\phi)$, which approximates the intensity observed when a uniform parallel beam of light refracts from a surface with a surface profile defined by ϕ (the '4' here is the wavenumber k of the light being considered, the geometric theory of catastrophes applies in the limit $k \to \infty$, see e.g. [5], but a moderate number is chosen here to aid numerical calculations). Though this reduces us to gradient fields, it is a profound demonstration of how catastrophes organise complex and universal patterns, one of the deepest successes of Thom's catastrophe theory and one which helped create the field of singular optics [4, 5]. One may compare the simulations here with some stunning photographs of optical catastrophes captured in [5].

6.1 Fold

Consider the system

$$f = \left(x_2 + x_1^2,\ x_2 + \alpha_1\right) \ . \tag{22}$$

The $\mathcal{B}$-$\mathcal{G}$ conditions to codimension $r = 1$ evaluate as

$$\begin{aligned} \mathcal{B}_1 &= 2x_1 \ , \\ \mathcal{G}_1 &= 2 \ . \end{aligned} \tag{23}$$

Hence there are full folds given by

$$f = \mathcal{B}_1 = 0 \quad \Rightarrow \quad x_1 = x_2 = \alpha_1 = 0 \ , \tag{24}$$

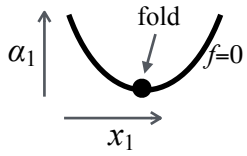

Figure 7: A simple fold in a non-gradient system (22).

shown as the fold of the curve of equilibria in fig. 7.

The system (22) defines a saddle-node. If we interchange the components $(f_1, f_2) \leftrightarrow (f_2, f_1)$ we obtain a saddle-focus, which as we saw in section 4 has higher codimension as a bifurcation class, the lowest of which is the Bogdanov-Takens bifurcation. Both are shown in fig. 8(i-ii), along with the image of a typical diffraction integral in (iii), given by $\int_{-\infty}^{-\infty} dx_1 \cos(4\phi)$ with $\phi = \frac{1}{3}x_1^3 + \alpha_1 x_1$, for which $f = \nabla\phi$ has a fold at the origin.

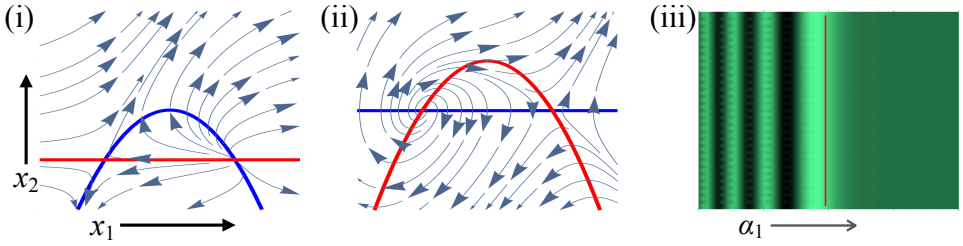

Figure 8: Phase portraits of (22) showing: (i) $(\dot{x}_1, \dot{x}_2) = f$ with a saddle-node, and (ii) $(\dot{x}_2, \dot{x}_1) = f$ with a saddle-focus, both plotted for $\alpha_1 = 1$. The intensity plot (iii) shows the typical Airy integral of diffraction around a fold. In (i)-(ii) the $\dot{x}_1$ and $\dot{x}_2$ nullclines are shown by red and blue curves, respectively, and in (iii) the red curve shows the fold set.

6.2 Cusp

Consider

$$f = \left(x_2 + \alpha_2 x_1 + x_1^3,\ x_2 + \alpha_1\right) \ , \tag{25}$$

and the $\mathcal{B}$-$\mathcal{G}$ conditions to codimension $r = 2$,

$$\begin{aligned} \mathcal{B}_1 &= \alpha_2 + 3x_1^2 \ , \\ \mathcal{B}_2 &= 6x_1 \ , \\ \mathcal{G}_{2i} &= \pm 6 \ . \end{aligned} \tag{26}$$

We can write the set of equilibria as $\alpha_1 = -x_2 = \alpha_2 x_1 + x_1^3$, which have folds at $\alpha_2 = -3x_1^2$, and a cusp at

$$f = \mathcal{B}_1 = \mathcal{B}_2 = 0 \quad \Rightarrow \quad x_1 = y_1 = \alpha_1 = \alpha_2 = 0\,. \tag{27}$$

The surface of equilibria is shown in fig. 9, with curves of folds intersecting at the cusp.

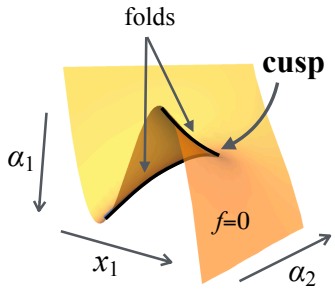

Figure 9: Unfolding of the cusp (25): the surface of equilibria, with folds intersecting at a cusp.

The phase portrait of (25) is shown in fig. 10(i), while interchanging the components of the field yields the same cusp underlying a higher codimension bifurcation involving foci, shown in fig. 10(ii). These cases have a node-saddle-node, and a saddle-focus-saddle, respectively, the nodes/foci being unstable; by changing signs it is easy to obtain corresponding cases with a saddle-node-saddle and a focus-saddle-focus, or with stable nodes/foci, the more important feature is that (i) forms a bifurcation class while (ii) has

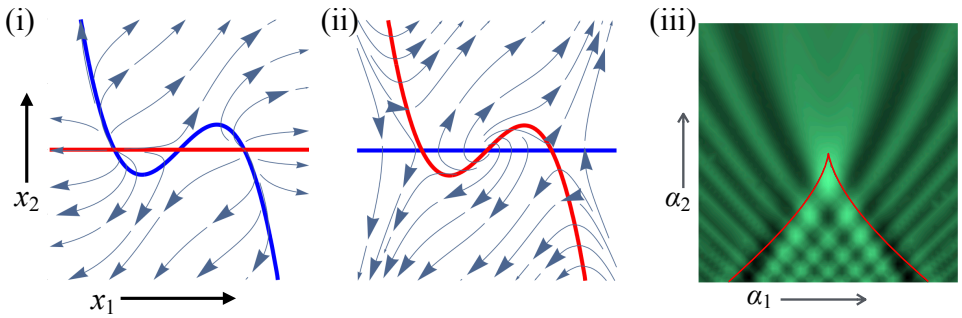

Figure 10: Phase portraits of (25) showing: (i) $(\dot{x}_1, \dot{x}_2) = f$ with two nodes and a saddle, and (ii) $(\dot{x}_2, \dot{x}_1) = f$ with two saddles and a focus, both plotted for $\alpha_1 = 0$, $\alpha_2 = -1$. The intensity plot (iii) shows the typical Pearcey integral of diffraction around a cusp.

higher codimension as a bifurcation class, similar to the Bogdanov-Takens case for the fold in section 6.1. In (iii) I show the image of a typical diffraction integral at a cusp, given by $\int_{-\infty}^{-\infty} dx_1 \cos(4\phi)$ with $\phi = \frac{1}{4}x_1^4 + \frac{1}{2}\alpha_2 x_1^2 + \alpha_1 x_1$, for which $f = \nabla\phi$ has a cusp at the origin.

6.3 Swallowtail

Next take

$$f = \left(x_2 + \alpha_3 x_1 + \alpha_2 x_1^2 + x_1^4,\ x_2 + \alpha_1\right) \ , \tag{28}$$

and the $\mathcal{B}$-$\mathcal{G}$ conditions to codimension $r = 3$,

$$\begin{aligned} \mathcal{B}_1 &= \alpha_2 + 2\alpha_3 x_1 + 4x_1^3 \ , \\ \mathcal{B}_2 &= 2\alpha_3 + 12x_1^2 \ , \\ \mathcal{B}_3 &= 24x_1 \ , \\ \mathcal{G}_{3i} &= 48 \ . \end{aligned} \tag{29}$$

We can write the set of equilibria as $\alpha_1 = -x_2 = \alpha_3 x_1 + \alpha_2 x_1^2 + x_1^4$, with folds at $\alpha_2 = -2\alpha_3 x_1 - 4x_1^3$, cusps at $\alpha_3 = -6x_1^2$, and so a swallowtail at

$$f = \mathcal{B}_1 = \mathcal{B}_2 = \mathcal{B}_3 = 0 \quad \Rightarrow \quad x_1 = y_1 = \alpha_1 = \alpha_2 = \alpha_3 = 0 \ . \tag{30}$$

These catastrophe sets are shown in $(\alpha_1, \alpha_2, \alpha_3)$ parameter space in fig. 11.

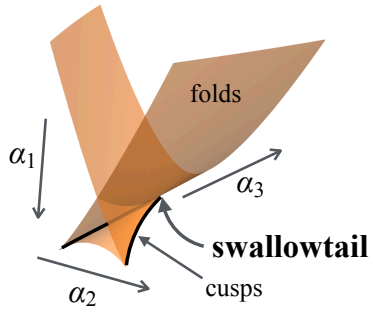

Figure 11: Unfolding of the swallowtail (28): the surface of folds, which crease along cusps, which intersect at the swallowtail point.

There is already little discussion of the swallowtail of a vector field in standard texts, though it does appear in applications, e.g. [23]. The phase portrait of fig. 11 is shown in fig. 12(i). Again, interchanging the components of the field yields the same catastrophe underlying a higher codimension

bifurcation involving foci, shown in fig. 12(ii), and (iii) shows the image of a typical diffraction integral near a swallowtail given by $\int_{-\infty}^{-\infty} dx_1 \cos(4\phi)$, with $\phi = \frac{1}{5}x_1^5 + \frac{1}{3}\alpha_3 x_1^3 + \frac{1}{2}\alpha_2 x_1^2 + \alpha_1 x_1$, for which $f = \nabla\phi$ has a swallowtail at the origin.

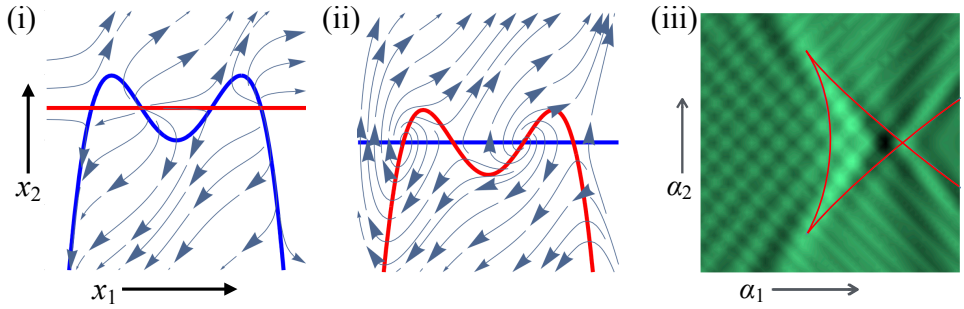

Figure 12: Phase portrait of (28) plotted for $\alpha_2 = 0$, $\alpha_3 = -2$, showing: (i) $(\dot{x}_1, \dot{x}_2) = f$ with $\alpha_1 = -\frac{1}{2}$, and (ii) $(\dot{x}_2, \dot{x}_1) = f$ with $\alpha_1 = \frac{1}{2}$. The intensity plot (iii) shows a typical integral of diffraction near a swallowtail with $\alpha_3 = -3$.

6.4 Butterfly

Lastly for these cases of corank 1, consider

$$f = \left(x_2 + \alpha_4 x_1 + \alpha_3 x_1^2 + \alpha_2 x_1^3 + x_1^5,\ x_2 + \alpha_1\right) \ , \tag{31}$$

and the $\mathcal{B}$-$\mathcal{G}$ conditions to codimension $r = 4$,

$$\begin{aligned}
\mathcal{B}_1 &= \alpha_2 + 2\alpha_3 x_1 + 3\alpha_4 x_1^2 + 5x_1^4 \ , \\
\mathcal{B}_2 &= 2\alpha_3 + 6\alpha_4 x_1^2 + 20 x_1^3 \ , \\
\mathcal{B}_3 &= 6\alpha_4 + 60 x_1^2 \ , \\
\mathcal{B}_4 &= 120 x_1 \ , \\
\mathcal{G}_{4i} &= \pm 1440 \ .
\end{aligned} \tag{32}$$

We can write the set of equilibria as $\alpha_1 = -x_2 = \alpha_4 x_1 + \alpha_3 x_1^2 + \alpha_2 x_1^3 + x_1^5$, with folds at $\alpha_2 = -2\alpha_3 x_1 - 3\alpha_4 x_1^2 - 5x_1^4$, cusps at $\alpha_4 = -10x_1^2$, and a butterfly at

$$\begin{aligned}
& f = \mathcal{B}_1 = \mathcal{B}_2 = \mathcal{B}_3 = \mathcal{B}_4 = 0 \\
\Rightarrow \quad & x_1 = y_1 = \alpha_1 = \alpha_2 = \alpha_3 = \alpha_4 = 0 \ .
\end{aligned} \tag{33}$$

To illustrate the catastrophe sets in $(\alpha_1, \alpha_2, \alpha_3, \alpha_4)$ parameter space we can choose different sections. Figure 13 shows 3-dimensional slices in $\alpha_4 = 0$ and $\alpha_3 = 0$. Figure 14(left) shows a slice through $\alpha_4 = -1$, in which the swallowtails are visible as points (which will collide at the butterfly when $\alpha_4 = 0$), while fig. 14(right) shows the surface of cusps in $(\alpha_2, \alpha_3, \alpha_4)$ space, which form a surface similar to fig. 11, but now creasing along curves of swallowtails that collide at the butterfly.

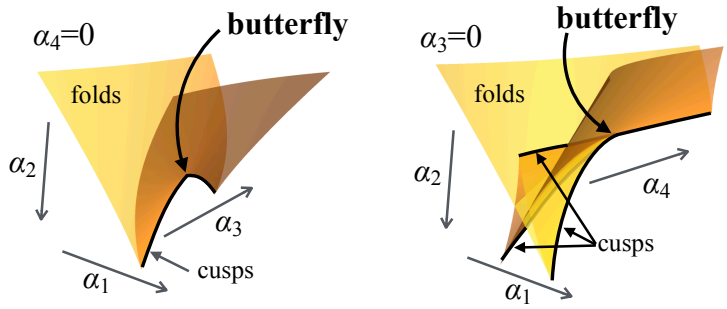

Figure 13: Representations of the butterfly unfolding, depicting the set of folds in sections $\alpha_4 = 0$ (left) and $\alpha_3 = 0$ (right) through $(\alpha_1, \alpha_2, \alpha_3, \alpha_4)$ parameter space.

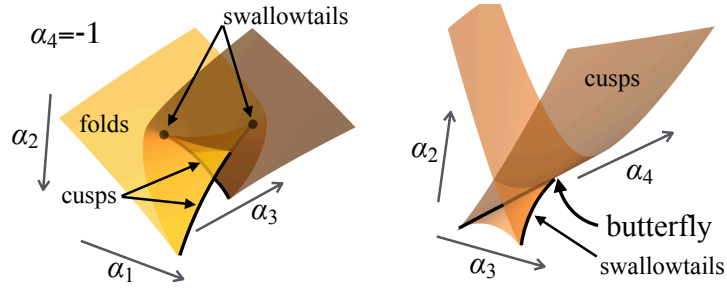

Figure 14: Representations of the butterfly unfolding, depicting the set of folds in the section $\alpha_4 = 1$ (left), and the set of cusps (right) in $(\alpha_2, \alpha_3, \alpha_4)$ space.

I am not aware of any study of the butterfly of a vector field in standard theoretical literature, but again it is beginning to appear in applications [7, 8, 17]. The phase portrait of (31) is shown in fig. 15(i), and in (ii) with the components of the field interchanged to yield the same catastrophe underlying a higher codimension bifurcation involving foci. Lastly, (iii) shows the image of a typical diffraction integral near a butterfly given by $\int_{-\infty}^{-\infty} dx_1 \cos(4\phi)$, with $\phi = \frac{1}{6}x_1^6 + \frac{1}{4}x^4 + \frac{1}{3}\alpha_3 x_1^3 + \frac{1}{2}\alpha_2 x_1^2 + \alpha_1 x_1$, for which $f = \nabla\phi$ has a butterfly at the origin.

The corank 1 catastrophes can be continued in a fairly obvious manner

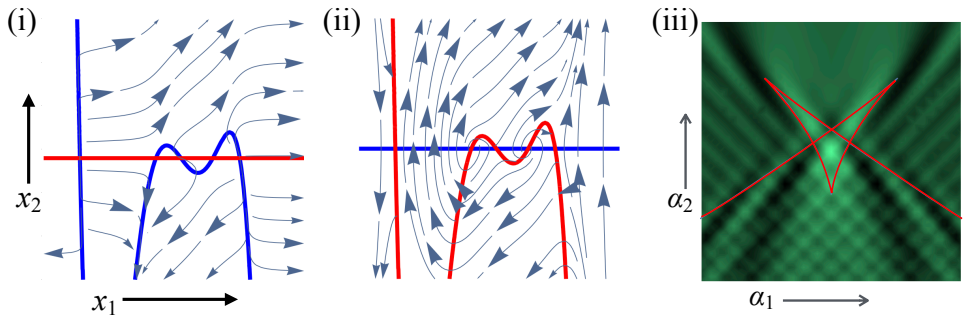

Figure 15: Phase portrait of (31) as (i) $(\dot{x}_1, \dot{x}_2) = f$ and (ii) $(\dot{x}_2, \dot{x}_1) = f$, both with $\alpha_1 = -\frac{1}{5}$, $\alpha_2 = 1$, $\alpha_3 = 2$, $\alpha_4 = -4$. The intensity plot (iii) shows a typical integral of diffraction near a butterfly with $\alpha_3 = 0$, $\alpha_4 = -3$.

to successively higher codimension. Let us move on to the richer corank 2 catastrophes. I will present the hyperbolic and elliptic cases, before giving a note on the distinction between them in section 6.7.

6.5 Hyperbolic

First take the hyperbolic umbilic, in a more convenient form for unfolding than in section 5,

$$f = \left(2x_1x_2 + \alpha_3 x_1 + \alpha_1,\ x_1^2 + x_2^2 + \alpha_4 x_1 + \alpha_2\right) \ . \tag{34}$$

The $\mathcal{B}$-$\mathcal{G}$ conditions evaluate as

$$\begin{aligned} \mathcal{B}_1 &= 4x_2^2 + 2\alpha_3 x_2 - 4x_1^2 - 2\alpha_4 x_1 \ , \\ \mathcal{B}^2_{1,k} &= \{\alpha_3 + 2x_2,\ 2x_1,\ \alpha_4 + 2x_1,\ 2x_2\} \ , \\ \mathcal{G}^2_{1,k} &= -4 \ . \end{aligned} \tag{35}$$

The sets of equilibria can be written as

$$(\alpha_1, \alpha_2) = -\left(2x_1x_2 + \alpha_3 x_1,\ x_1^2 + x_2^2 + \alpha_4 x_1\right) \ .$$

A good way to plot the fold surfaces where $\mathcal{B}_1 = 0$ is to re-parameterise by letting $(x_1, x_2) = -\frac{1}{4}(\alpha_4, \alpha_3) \pm \frac{1}{4}\sqrt{\alpha_4^2 - \alpha_3^2}\,(\cosh\theta, \sinh\theta)$ for $\theta \in \mathbb{R}$. This produces the two-sheeted surface depicted for $\alpha_3 = 0$ in fig. 16 (this simple form is why we take (34) instead of (17) here, but the same can be achieved by a coordinate change).

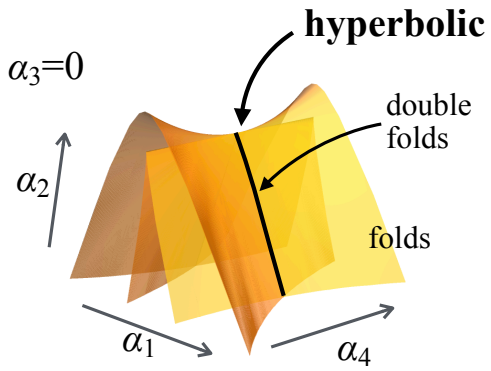

Figure 16: The hyperbolic umbilic unfolding plotted for $\alpha_3 = 0$, showing the fold set, with two sheets that meet along a family of double-folds emanating from the hyperbolic point.

The two sheets meet along a family of double-folds where $\alpha_3 = \pm\alpha_4$, such that in the (x, y) plane folds occur at simultaneously at $(x_1, x_2) = \frac{1}{4}(\pm\alpha_3, \alpha_3)$, where $\alpha_2 = \pm\alpha_1 = \frac{1}{8}\alpha_3^2$. One sheet creases along a family of cusps, but they are not full for the form (34) so I omit them here, and will remark on them further in section 6.7.

Example phase portraits are shown in fig. 17(i-ii). The hyperbolic can have two saddles, and two nodes or foci of opposite stability in (i) or (ii) respectively (and the saddle-node or saddle-focus pairs can annihilate in folds to leave just two or zero equilibria, as we saw in section 5).

The diffraction integral shown in fig. 17(iii) is a numerical integration of $\int_{-\infty}^{-\infty} dx_1 dx_2 \cos(4\phi)$, with $\phi = \alpha_1 x_1 + \alpha_2 x_2 + \alpha_4 x_1 x_2 + x_1^2 x_2 + \frac{1}{2}\alpha_3 x_1^2 + \frac{1}{3}x_2^3$.

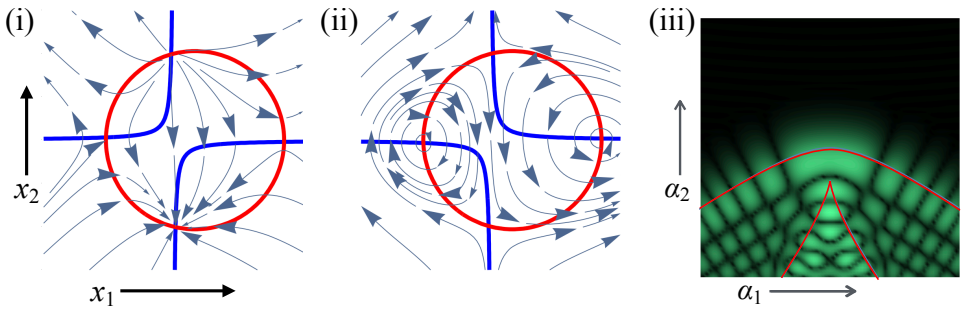

Figure 17: Phase portrait of (34) plotted for $\alpha_1 = \frac{1}{5}$, $\alpha_2 = -4$, $\alpha_3 = 0$, $\alpha_4 = -1$, showing: (i) $(\dot{x}_1, \dot{x}_2) = f$, and (ii) $(\dot{x}_2, \dot{x}_1) = f$. The intensity plot (iii) shows a diffraction integral near a hyperbolic umbilic with $\alpha_3 = 2$, $\alpha_4 = 0$.

6.6 Elliptic

The last case I will illustrate here is the elliptic umbilic, simply changing a sign from (34). Take the system

$$f = \left(2x_1x_2 + \alpha_3x_1 + \alpha_1,\ x_1^2 - x_2^2 + \alpha_4x_1 + \alpha_2\right)\ . \tag{36}$$

The $\mathcal{B}$-$\mathcal{G}$ conditions evaluate as

$$\begin{aligned}\mathcal{B}_1 &= -4x_2^2 - 2\alpha_3x_2 - 4x_1^2 - 2\alpha_4x_1\ ,\\ \mathcal{B}^2_{1,k} &= \{\alpha_3 + 2x_2,\ 2x_1,\ \alpha_4 + 2x_1,\ -2x_2\}\ ,\\ \mathcal{G}^2_{1,k} &= 4\ .\end{aligned} \tag{37}$$

The sets of equilibria can be written as

$$(\alpha_1, \alpha_2) = -\left(2x_1x_2 + \alpha_3x_1,\ x_1^2 - x_2^2 + \alpha_4x_1\right)\ .$$

To plot the fold surfaces where $\mathcal{B}_1 = 0$ we can re-parameterise by letting $(x_1, x_2) = -\frac{1}{4}(\alpha_4, \alpha_3) + \frac{1}{4}\sqrt{\alpha_4^2 - \alpha_3^2}\,(\cos\theta, \sin\theta)$ for $\theta \in [0, 2\pi)$. This produces the deltoid surface depicted for $\alpha_3 = 0$ in fig. 18. The deltoid clearly has three families of cusps, but similar to the hyperbolic they are not full for the form (36), so I leave these to a remark in section 6.7.

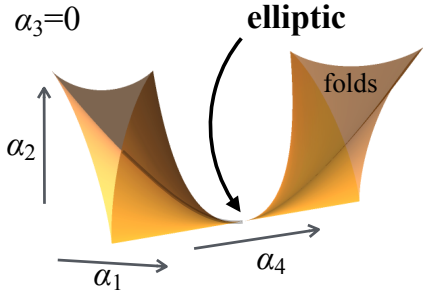

Figure 18: The elliptic umbilic unfolding plotted for $\alpha_3 = 0$, showing the fold set, creasing along three families of cusps emanating from the elliptic point.

Example phase portraits are shown in fig. 19(i-ii). The elliptic can have three saddles and one node/focus, or one saddle and three nodes/foci (and a saddle-node or saddle-focus pair can annihilate in a fold to leave at last two equilibria, both of either saddle type, or both of node/focus type, as we saw in section 5).

The diffraction integral shown in fig. 19(iii) is a numerical integration of $\int_{-\infty}^{-\infty} dx_1dx_2\cos(4\phi)$, with $\phi = \alpha_1x_1 + \alpha_2x_2 + \alpha_4x_1x_2 + x_1^2x_2 + \frac{1}{2}\alpha_3x_1^2 - \frac{1}{3}x_2^3$.

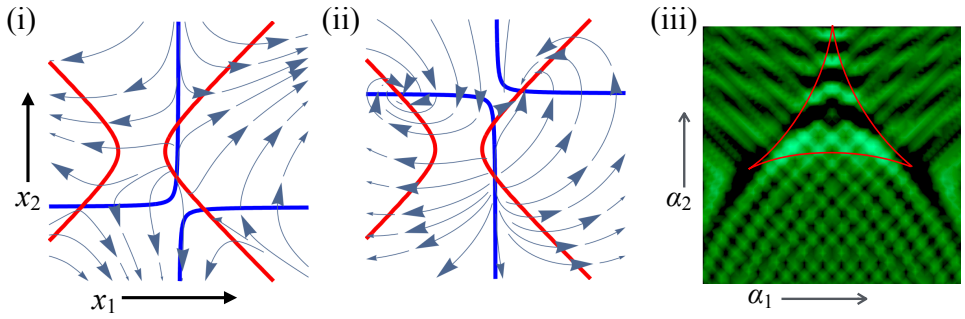

Figure 19: Phase portrait of (36) plotted for $\alpha_1 = \frac{1}{10}$, $\alpha_2 = \frac{3}{5}$, $\alpha_3 = 3$, $\alpha_4 = 2$, showing: (i) $(\dot{x}_1, \dot{x}_2) = f$, and (ii) $(\dot{x}_2, \dot{x}_1) = f$. The intensity plot (iii) shows a diffraction integral near an elliptic umbilic with $\alpha_3 = 4$, $\alpha_4 = 0$.

6.7 Note on the umbilics

The means to classify singularities as either hyperbolic or elliptic is somewhat obscure in many texts, but is well described in [21] in a manner applicable to the planar vector fields above. The type of a quadratic form $f_1 = \frac{1}{2}ax_1^2 + bx_1x_2 + \frac{1}{2}cx_2^2$ can be found from its Hessian matrix $S = \frac{\partial^2 f_1}{\partial x_i \partial x_2} = \begin{pmatrix} a & b \\ b & c \end{pmatrix}$; the function is hyperbolic, elliptic, or parabolic, if the determinant $|S|$ is negative, positive, or zero, respectively. To find the type of a planar quadratic form $f = (f_1, f_2)$, we first form a combination of the Hessians $S_{\lambda_1\lambda_2} = \lambda_1 \frac{\partial^2 f_1}{\partial x_i \partial x_j} + \lambda_2 \frac{\partial^2 f_2}{\partial x_i \partial x_2}$, then consider the determinant $|S_{\lambda_1\lambda_2}|$ as a quadratic form in (λ_1, λ_2), and hence form the Hessian $S = \frac{\partial^2 f_1}{\partial \lambda_i \partial \lambda_j}$, to again find that the function is hyperbolic, elliptic, or parabolic, if the determinant $|S|$ is negative, positive, zero, respectively. For the geometric interpretation of how this characterises the way a function spans the space of quadratic forms see [21].

Calculating directly for the umbilics in section 6.5-6.6, for (34) we obtain a hyperbolic, since

$$S_{\lambda_1\lambda_2} = \begin{pmatrix} \lambda_2 & \lambda_1 \\ \lambda_1 & \lambda_2 \end{pmatrix} \quad \Rightarrow \quad |S_{\lambda_1\lambda_2}| = \lambda_2^2 - \lambda_1^2$$
$$\& \qquad S = \begin{pmatrix} -1 & 0 \\ 0 & 1 \end{pmatrix} \quad \Rightarrow \quad |S| = -1 \ < \ 0 \,, \tag{38}$$

and for (36) we obtain an elliptic, since

$$S_{\lambda_1\lambda_2} = \begin{pmatrix} \lambda_2 & \lambda_1 \\ \lambda_1 & -\lambda_2 \end{pmatrix} \quad \Rightarrow \quad |S_{\lambda_1\lambda_2}| = -\lambda_2^2 - \lambda_1^2$$
$$\& \qquad S = \begin{pmatrix} -1 & 0 \\ 0 & -1 \end{pmatrix} \quad \Rightarrow \quad |S| = 1 \ > \ 0 \, . \tag{39}$$

I remarked in section 6.5-6.6 that the cusps observed on the fold sets are not full for the forms of umbilic given here, so they cannot be found using the condition $\mathcal{B}_2 = 0$. They can be made full by adding certain terms to (34) and (36), but this considerably complicates the analysis to show the unfoldings. A complete analysis will form part of a more far reaching theory currently in draft, which will seek to fully bridge the gap between the underlying catastrophes, which are merely a methodological tool for finding bifurcations, and the full rigour of bifurcation theory.

7 Closing remarks

I stated in the introduction that underlying catastrophes aim to bring the simplicity of catastrophe theory back into bifurcation theory, and render it more amenable to application without altering the theory itself. It must be noted that in this respect, underlying catastrophes seek only to be a methodological tool, and in this paper I have sought to not only explain their working, but also highlight cases where they do not fully capture bifurcation classes. As mentioned at the end of section 6, it seems that a deeper theoretical development should be possible that closes this gap between the method of underlying catastrophes and the theory of vector field bifurcations; this work is currently in draft with P.C.C.R. Pereira and expected to appear soon.

This forthcoming work aims to lay down a more rigorous theory for the underlying catastrophes, and make the necessary extensions to identify bifurcation classes. Future work will also look more closely at the umbilics, to prove the form of their unfoldings and derive their different bifurcation classes, as these seem to be new to the bifurcation theory of vector fields. It is hoped that such work will also fully extend the $\mathcal{B}$-$\mathcal{G}$ conditions to the umbilics, as beyond the hyperbolic and elliptic shown here, there lie also the parabolic and symbolic umbilics, and higher codimensions, well known in catastrophe and singularity theory but unknown in general vector fields. It may also be possible to extend the concept of underlying catastrophes to global dynamics by applying them to return maps, and some steps in this

direction are taken by looking at catastrophes of the 'displacement map', though in the context of averaging theory, in [16].

Acknowledgements

In developing these ideas I am indebted to generous conversations with F. Dumortier and D. Chillingworth, and to ongoing work with P. Pereira with whom many of these concepts have become clearer, and to many years of inspiring interactions with Marco Antonio Teixeira whose geometrical insights deeply influenced the conception of underlying catastrophes.

References

[1] F. A. Al Saadi, A. R. Champneys, and M. R. Jeffrey. Wave-pinned patterns for cell polarity – a catastrophe theory explanation. *SIAM Journal on Applied Dynamical Systems*, 23(1):721–47, 2024.

[2] V. I. Arnold, V. S. Afrajmovich, Y. S. Il'yashenko, and L. P. Shil'nikov. *Dynamical Systems V: Bifurcation Theory and Catastrophe Theory*. Encyc. of Mathematical Sciences. Springer Verlag, 1994.

[3] V. I. Arnol'd, A. N. Varchenko, and S. M. Gusein-Zade. *Singularities of Differentiable Maps*. Birkhäuser, 1985.

[4] M. V. Berry. In support of catastrophe theory. *Nature*, 270:382–3, 1977.

[5] M. V. Berry and C. Upstill. Catastrophe optics: morphologies of caustics and their diffraction patterns. *Progress in Optics*, XVIII:257–346, 1980.

[6] J. M. Boardman. Singularities of differentiable maps. *Publications mathématiques de l'IHÉS.*, 33:21–57, 1967.

[7] M. Chrilus-Bruckner, A. Doelman, P. van Heijster, and J. D. M. Rademacher. Butterfly catastrophe for fronts in a three-component reaction–diffusion system. *J. Nonlinear Sci.*, 25:87–129, 2015.

[8] J. Cisternas, K. Rohe, and S. Wehner. Reaction–diffusion fronts and the butterfly set. *Chaos*, 30(113138):1–14, 2020.

[9] F. Dumortier, R. Roussarie, J. Sotomayor, and H. Zoladek. *Bifurcations of Planar Vector Fields: Nilpotent Singularities and Abelian Integrals*. Springer-Verlag, 1991.

[10] M. Golubitsky and V. Guillemin. *Stable Mappings and their Singularities*. Springer-Verlag, 1973.

[11] J. Guckenheimer. Bifurcation and catastrophe. In M.M. Peixoto, editor, *Dynamical Systems*, pages 95–109. Academic Press, 1973.

[12] M. P. Holl, A. J. Archer, and U. Thiele. Efficient calculation of phase coexistence and phase diagrams: application to a binary phase-field-crystal model. *J. Phys: Condens. Matter*, 33(115401):1–15, 2021.

[13] M. R. Jeffrey. Catastrophe conditions for vector fields in $\mathbb{R}^n$. *J. Phys. A: Math. Theor. Special Issue on Claritons and the Asymptotics of Ideas: the Physics of Michael Berry*, 55(464006):1–25, 2022.

[14] M. R. Jeffrey. Elementary catastrophes underlying bifurcations of vector fields and PDEs. *Nonlinearity*, 37(085005):1–22, 2024.

[15] M. R. Jeffrey. Underlying catastrophes: umbilics and pattern formation. *São Paulo Journal of Mathematical Sciences, Special Volume on Stability and Bifurcation - Memorial Issue dedicated to Jorge Sotomayor*, 2024.

[16] M. R. Jeffrey, D. D. Novaes, and P. C. C. R. Perreira. Averaging theory and catastrophes: The persistence of bifurcations under time-periodic perturbations. *submitted*, 2024.

[17] O. Y. Khachay and P. A. Nosov. On some numerical integration curves for PDE in neighborhood of "butterfly" catastrophe point. *Ural Math. Journal*, 2(2):127–40, 2016.

[18] Y. A. Kuznetsov. *Elements of Applied Bifurcation Theory*. Springer, 3rd Ed., 2004.

[19] J. Martinet. *Singularities of Smooth Functions and Maps*. LMS Lect. Notes 58. Cambridge Univ. Press, 1982.

[20] J. N. Mather. On Thom-Boardman singularities. In M. M. Peixoto, editor, *Dynamical Systems*, pages 233–248. Academic Press, 1973.

[21] J. Montaldi. *Singularities, Bifurcations and Catastrophes*. Cambridge Univ. Press, 2021.

[22] T. Poston and I. N. Stewart. *Catastrophe theory and its applications*. Dover, 1996.

[23] K. Rohe, J. Cisternas, and S. Wehner. Competing ternary surface reaction $CO + O_2 + H_2$ on Ir(111). *Proc. R. Soc. A*, 476(20190712):1–16, 2023.

[24] R. Thom. Topological models in biology. *Topology*, 8:313–35., 1969.

[25] R. Thom. *Structural stability and morphogenesis*. Benjamin-Addison Wesley, translation by D.H.Fowler, original in French 1972 edition, 1975.